Electrochimica Acta 258 (2017) 1201–1207

Contents lists available at ScienceDirect

Electrochimica Acta

journal homepage: www.elsevier.com/locate/electacta

A tin-plated copper substrate for efficient cycling of lithium metal in an anode-free rechargeable lithium battery

Sheng S. Zhang [a, *], Xiulin Fan [b], Chunsheng Wang [b]

[a] Electrochemistry Branch, RDRL-SED-C, Sensors and Electron Devices Directorate, U.S. Army Research Laboratory, Adelphi, MD 20783-1138, USA
[b] Department of Chemical and Biomolecular Engineering, University of Maryland, College Park, MD 20742, USA

ARTICLE INFO

Article history:
Received 26 October 2017
Received in revised form
21 November 2017
Accepted 24 November 2017
Available online 26 November 2017

Keywords:
Lithium battery
Electroless tin plating
Li-Sn alloy
Li plating
Coulombic efficiency

ABSTRACT

Adhesion of Li plating to electrode substrate and chemical stability of plated Li against electrolyte components are two essential factors affecting the cycling performance of Li metal in a rechargeable Li battery. Poor adhesion results in high contact resistance and further the formation of dead Li. Aiming to improve the adhesion of Li plating to Cu substrate, we plate a very thin tin layer as the primer for Li plating on the Cu substrate. By this way, Li metal is first reacted with tin to form a Li-Sn alloy, and then Li is cycled on resultant Li-Sn alloy so that the Li-Sn alloy functions as an "electric glue" to electrically connect the Li plating and Cu substrate. Attributed to the strong affinity between Li and Li-Sn alloy, the pre-plated tin layer is shown not only to enhance the adhesion of the plated Li to electrode substrate but also to improve the morphology of Li plating. Using a 1.0 m (molality) $LiPF_6$ 1:4 (wt.) fluoroethylene carbonate/ethylmethyl carbonate electrolyte, in this paper the effect of the tin primer layer on the Li cycling performance in a Li/Cu cell and a Cu/$LiNi_{0.85}Co_{0.10}Al_{0.05}O_2$ cell is demonstrated and discussed.
Published by Elsevier Ltd.

1. Introduction

Lithium (Li) metal is capable of providing the highest energy density as the anode material of rechargeable batteries due to its light atomic weight (6.941 g mol^{-1}) and low standard electrode potential (−3.0401 V vs. SHE, standard hydrogen electrode). However, previous attempts in developing rechargeable Li batteries were unsuccessful due to the poor cyclability and inferior safety of metal Li. It is generally believed that the poor cyclability is due to the high reactivity of metal Li with electrolyte components and the inferior safety originates from the dendrite growth of Li metal in charging process [1,2]. In an accident, excess amount of Li metal is identified to be the most severe hazard because it immediately becomes a strong fuel once it is exposed to air or water. Therefore, reducing excessive Li metal is of particular significance in not only increasing the energy density but also improving the safety of Li batteries. In efforts to reduce the amount of Li metal, a "Li-free battery" concept has been proposed by using a Li-rich cathode and a Cu foil as the anode current collector to enable the Li metal being *in-situ* plated onto the Cu substrate [3,4]. The key to success of this concept is the efficient and stable cycling of Li metal on the Cu substrate, which essentially relies on two factors of (1) the chemical stability of Li metal against electrolyte components and (2) the adhesion of Li plating to the Cu substrate.

In efforts to reduce parasitic reactions between Li deposit and electrolyte components, particular interest has been placed in highly concentrated electrolyte solutions [5–8] and fluorinated electrolyte components in forms of salt [6,7,9], solvent [10], and additive [11,12]. In the former, Li metal is stabilized by a dramatic decrease in the number of free solvent molecules as a result of the coordination between Li^+ ions and solvent molecules (namely the solvation); In the latter, some of fluorine atoms in the fluorinated compounds are combined with Li^+ ions, forming a robust solid electrolyte interphase (SEI) to protect Li metal from parasitic reactions with the solvents. In this regard, lithium bis(fluorosulfonyl) imide [6,7,9] and fluoroethylene carbonate [10] are shown particular ability to release free fluorine anions that are stably incorporated into the protective SEI. In addition to reducing parasitic reactions, optimizing electrolyte salt and solvent [13,14] as well as employing electrolyte additive [15–18] are shown to improve the morphology of Li plating and hence improve the cycling efficiency of Li metal.

Poor electrical contact between Li plating and Cu substrate as well as between Li deposits is one of the most important causes for

* Corresponding author.
E-mail addresses: shengshui.zhang.civ@mail.mil, shengshui@gmail.com (S.S. Zhang).

https://doi.org/10.1016/j.electacta.2017.11.175
0013-4686/Published by Elsevier Ltd.

forming mossy dead Li, and it is believed to be the most challenging for "Li-free battery" due to the limited amount of Li^+ ions available from the cathode. Previous works on improving the adhesion of Li plating to electrode substrate are mainly through enhancing the effective area or lithiophilicity of the electrode substrate, including (1) replacement of Cu foil with a carbon substrate having large specific surface area, such as a porous carbon-fiber paper [19] and a porous graphene network [20], to reduce the electrode's local current density, and (2) surface modification of Cu foil, such as by slurry-coating a functional graphene layer [21], a nitrogen-doped graphene layer [22], or a highly conductive carbon primer layer [23] as well as by chemical vapor depositing graphene-carbon nanotube clusters [24], to increase the electrode's lithiophilicity. All the above approaches have shown inferior initial reversibility either due to the catalytic reduction of electrolyte solvents on the fresh surface/edge sites of carbon granules or due to the reduction of organic functional groups on the surface of carbon materials [25].

Aiming to reduce the initial irreversibility and improve the adhesion of Li plating to electrode substrate, in this work we employed an electroless tin plating technique to pre-plate a very thin tin layer onto the surface of an existing Cu substrate. Thus, the Li metal is first deposited onto the tin surface and instantly reacted with tin to form a Sn-Li alloy, and the next Li are plated and stripped on the Sn-Li alloy surface. Due to the chemical similarity between Li metal and Sn-Li alloy (and hence the excellent affinity), the pre-plated tin (which later was *in-situ* converted to Sn-Li alloy) primer layer is shown to function as an "electric glue" electrically connecting the plated Li and Cu substrate, resulting in improved Li cycling performance. In this paper, the effect of the pre-plated tin primer layer on the cycling performance of Li metal in a Li/Cu cell and a Cu/$LiNi_{0.85}Co_{0.10}Al_{0.05}O_2$ cell are evaluated and discussed.

2. Experimental

Liquid tin 421, a water solution consisting by weight of 4% tin tetrafluoroborate, 3% sodium hypophosphite 8%, fluoroboric acid, 8% thiourea, and 1% boric acid, was purchased from MG Chemicals (Ontario, Canada). In order to plate tin metal on single side, one side of the Cu foil was covered using a 3 M packing tape, and then immersed into a 0.5 M HCl solution for 1 min to remove native oxides on the surface. The cleaned Cu foil was dipped into a liquid tin bath at room temperature for 30 s, which immediately plated a bright-gray tin layer on the Cu surface. Resultant tin-plated Cu (hereafter referred to "Sn-Cu") foil was rinsed in deionized water and dried in air. To be tested as the electrode substrate for Li plating, the pristine Cu foil and Sn-Cu foil were punished into circular disks having a 1.98 cm^2 area (i.e., in a 5/8 inch diameter). A Li foil and a $LiNi_{0.85}Co_{0.10}Al_{0.05}O_2$ (NCA) cathode having an areal specific capacity of 1.0 mAh cm^{-2} (equal to 155 mAh g^{-1} NCA) were respectively punished into 1.27 cm^2 disks (i.e., in a ½ inch diameter). Prior to use, the NCA cathode was dried at 110 °C under vacuum for 15 h.

A solution consisting of 1.0 m (molality) $LiPF_6$ dissolved in a 1:4 (wt.) mixture of fluorethylene carbonate (FEC) and ethyl methyl carbonate (EMC) was used as the electrolyte. BR2335-sized Li/M and M/NCA (M = Li, Cu, or Sn-Cu) coin cells were assembled and filled with 40 μL electrolyte by using the electrodes described above and a Celgard 2400 membrane as the separator. On a Maccor Series 4000 tester, the Li/M cells were cycled at 0.5 mA cm^{-2} by plating Li metal to a fixed capacity of 0.50 mAh cm^{-2} and striped the cell to 1.0 V for 10 cycles, followed by changing the stripping limit voltage to 0.3 V afterward; The M/NCA cells were cycled at 0.1 mA cm^{-2} between 3.0 V and 4.2 V for 2 cycles, followed by cycling at 0.5 mA cm^{-2} for the rest.

Crystallographic structure of Sn plating was characterized by X-ray diffraction (XRD) using a D8 Advance X-ray diffraction (Bruker AXS, WI, USA) with a Cu Kα radiation source. Morphology of the Sn plating and Li plating was observed on a scanning electron microscopy (SEM, Hitachi SU-70). Ac-impedance of the cells was measured by a SI 1260 Impedance/Gain-Phase Analyzer in combination with a Solartron SI 1287 Electrochemical Interface in the frequency from 1.0×10^5 Hz to 0.01 Hz using an ac oscillation of 10 mV amplitude. The Li-plated Cu and Sn-Cu electrodes were harvested, rinsed with dimethyl carbonate, and dried in an argon-filled glovebox, followed by the SEM observation. In order to observe the cross-sectional view, the electrode sample with Li deposits was cut using a plastic scissor.

3. Results and discussion

A liquid tin-421 (MG Chemicals, Ontario, Canada) was used for electroless tin plating. While actual reactions are rather complicated, the general reactions for electroless tin plating in the presence of thiourea can be expressed by eqn. (1) and eqn. (2) [26].

$$Sn^{2+} + H_2PO_2^- + H_2O \rightarrow Sn + H_2PO_3^- + 2H^+ \quad (1)$$

$$Cu + Sn^{2+} + 4CS(NH_2)_2 \rightarrow Cu[CS(NH_2)_2]_4^{2+} + Sn \quad (2)$$

In eqn. (1), $H_2PO_2^-$ anions serve as the reducing agent to reduce Sn^{2+}, and in eqn. (2) metal Cu displaces Sn^{2+} to produce metal Sn as a result of a significant decrease in the standard Cu/$Cu[CS(NH_2)_2]_4^{2+}$ reduction potential by thiourea. According to the parameters (temperature and time) suggested by the vendor [27], a very thin tin layer (not more than 0.1 μm) was plated onto the Cu surface by immersing a cleaned Cu foil into the liquid tin bath at room temperature for 30 s. Preliminary characterizations of the Sn-Cu foil are presented in Fig. 1. Apparently, the Sn metal is plated in the form of a bright-gray, uniform, and dense layer (Fig. 1a). However, a detailed observation by SEM reveals that the tin plating layer is rather porous (Fig. 1b), which is because the amount of tin is too low to fully cover the Cu surface. Fig. 1c shows XRD pattern of the tin plating layer compared with those of the pristine Cu foil and standard Sn metal. It can be seen that the XRD pattern of the tin plating layer is composed mainly of the peaks of Cu and Sn metals in addition to trace amount of Sn-Cu alloys, as indicated by two small XRD peaks marked by the black triangles. The strong intensity of Cu diffusion peaks reveals that the tin plating layer is so thin that the X-ray can easily penetrate through the tin plating layer.

The tin plating layer is further characterized by energy-dispersive X-ray spectroscopy (EDS), as shown in Fig. 2. On the surface (Fig. 2a–d), both the Cu and Sn elements are obviously visible. In particular, the Cu element has much more populations than the Sn element (compare Fig. 2b and c), and numbers of Sn elements are distributed into the Cu matrix (see Fig. 2d), suggesting that (1) the tin-plating layer is very thin, and (2) some of Sn elements are combined with Cu to form a Sn-Cu alloy. Compared with Sn, Cu is extremely excessive. According to the Sn-Cu binary phase diagram [28], in such a condition the most possible stoichiometric alloys would be Cu_3Sn, $Cu_{10}Sn_3$, and $Cu_{41}Sn_{11}$. On the cross-sectional view (Fig. 2e–h), majority of Sn elements are distributed in the Cu matrix with only small portion of Sn elements being present as their alone (Fig. 2h). This observation indicates that in the Sn-Cu foil, the Sn elements are present in two forms of Sn metal and Sn-Cu alloy. The presence of Sn-Cu alloys is believed to be very helpful for mitigating the migration of Sn into Li deposits over time.

The effect of the pre-plated tin primer layer on Li plating and stripping was studied by galvanostatically cycling a Li/Cu cell and a Li/Sn-Cu cell. In this experiment, a 1.0 m $LiPF_6$ 1:4 (wt.) FEC/EMC electrolyte was used because FEC is known to be a favorable solvent or additive for the formation of robust SEI on the surface of anode

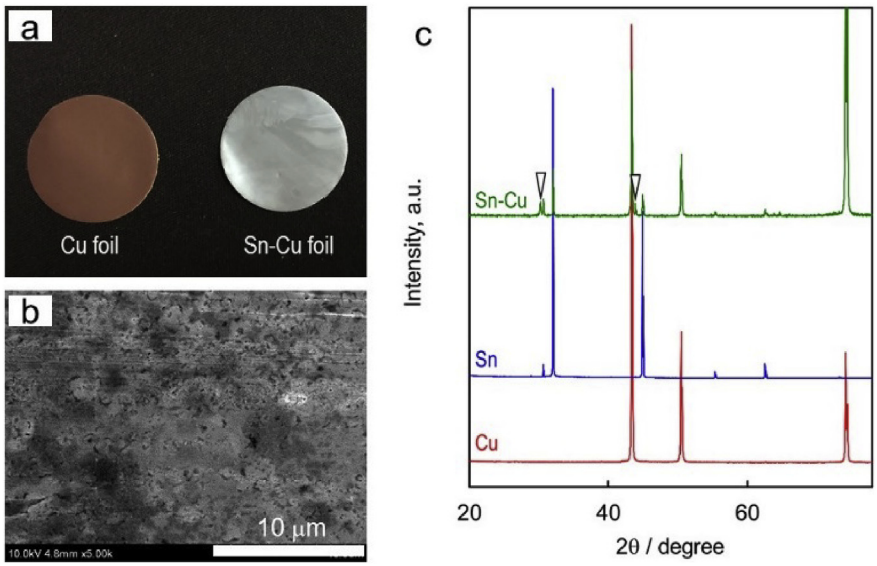

Fig. 1. (a) Digital photo of Cu and Sn-Cu foils, (b) SEM image of the surface of Sn-Cu foil, and (c) XRD patterns of Cu, Sn, and Sn-Cu foils.

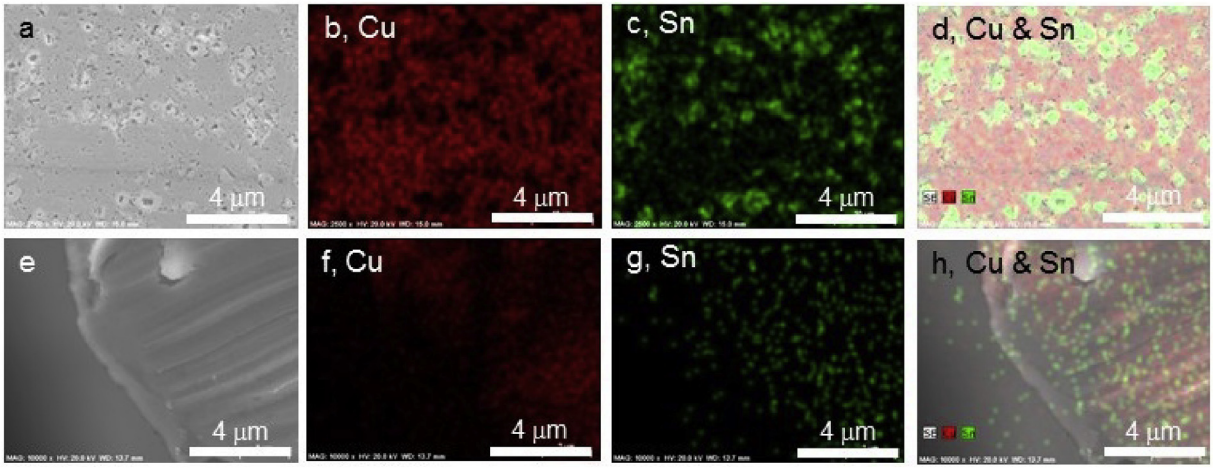

Fig. 2. EDS analysis on the surface (a–d) and cross-section (e–h) of Sn-Cu foil, showing the interested area (a, e), and elemental mapping of Cu (b, f), Sn (c, g), and both of Cu and Sn (d, h).

materials such as Li metal, graphite and silicon [10,12], and a testing schedule with relatively low Li plating capacity (0.5 mAh cm^{-2}) was used in order to highlight the impact of the tin primer layer on the Li cycling efficiency [29]. Fig. 3a and Fig. 3b show voltage profiles of the 1st and 2nd cycles, respectively. In the 1st plating (Fig. 3a), both the Li/Cu and Li/Sn-Cu cells consume small amount of capacity above 0 V vs. Li/Li^+ before reaching the potential for Li plating. In addition to the irreversible capacity used for the SEI formation, the initial capacity above 0 V in the Li/Cu cell is due to the irreversible reduction of native oxides (CuO and Cu_2O_2), and that in the Li/Sn-Cu cell is mainly attributed to the formation of Li-Sn alloy. For the potential of Li nucleation, the Li/Cu cell presents as a sharp peak while the Li/Sn-Cu cell shows a smooth bend (see Fig. 3a). This is because in the Li/Sn-Cu cell, Li metal is nucleated on the Li-Sn alloy, and Li metal has much stronger affinity to Li-Sn alloy as compared with the pristine Cu. The strong affinity between Li metal and Li-Sn alloy is well verified by the smaller over-potentials of Li plating and stripping in the Li/Sn-Cu cell as observed from Fig. 3a and b. In the 1st Li-stripping, the Li/Sn-Cu cell has lower capacity, leading to an inferior coulombic efficiency (CE, 70.8% vs. 79.1% of the Li/Cu cell) because not all Li atoms in the Li-Sn alloy can be electrochemically dealloyed in the subsequent charging step [30–33]. In the 2nd cycle (Fig. 3b), the CEs of both cells are increased and approached nearly same value (~90%).

The effect of Li-stripping ending voltage on Li cycling performance is illustrated in Fig. 3c. In the initial 10 cycles, the Li/M cells were stripped to 1.0 V. In this case, the Sn metal not only serves as the primer layer for Li plating but also acts as the active material for Li storage through the Li alloy-dealloy reaction. During this period, the CE of the Li/Sn-Cu cell gradually increases and eventually exceeds the control cell by 2–3%. Starting from the 11th cycle, the ending voltage for Li stripping was changed to 0.3 V below which the Li-Sn alloy stably retains and serves as the electrode substrate (primer layer) for Li plating. Compared with the control cell, the Li/Sn-Cu cell constantly exhibits 2–3% higher CEs except for the 11th cycle (CE = 88.1%) at which the ending voltage for Li stripping was changed from 1.0 V to 0.3 V so that some Li is permanently trapped in the form of Li-Sn alloy. It can be seen from Fig. 3c that in addition to the higher CEs, the Li/Sn-Cu cell showed better cycling stability.

In order to understand the superiority of the Sn-Cu foil in

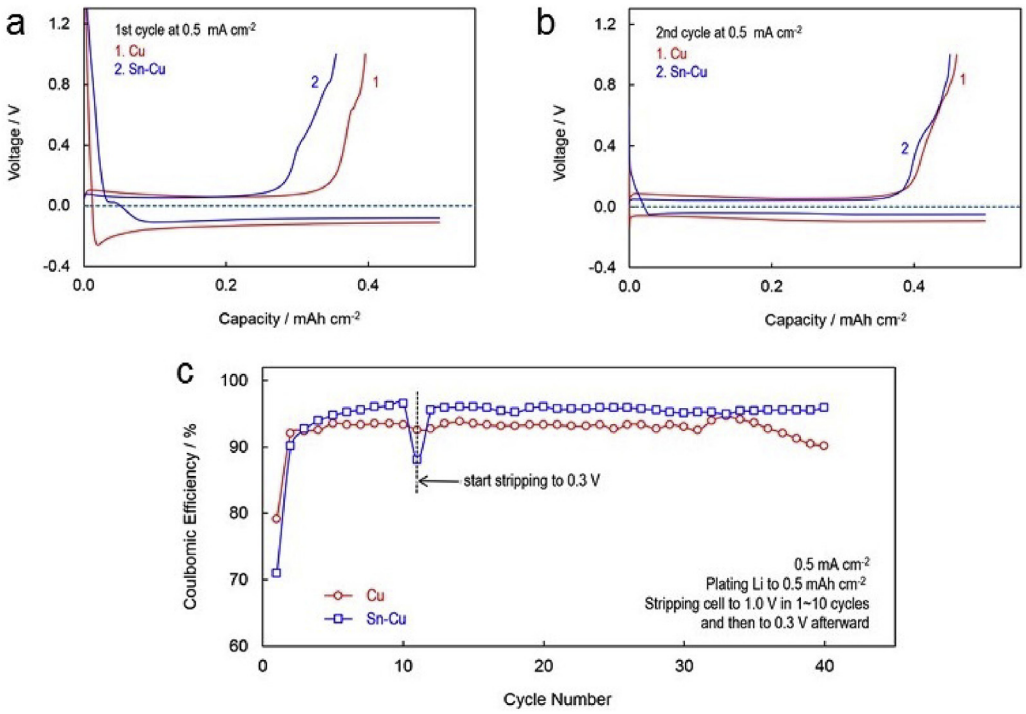

Fig. 3. Electrochemical characteristics of Li metal on Cu and Sn-Cu foils, which were recorded at 0.5 mA cm^{-2} by plating Li to 0.5 mAh cm^{-2} and striping the cell's voltage to 1.0 V or 0.3 V. (a) Voltage-capacity profile in the 1st cycle, (b) voltage-capacity profile in the 2nd cycle, and (c) plot of coulombic efficiency vs. cycle number.

facilitating Li plating, morphologies of the Li plating on the pristine Cu foil and Sn-Cu foil are compared in Fig. 4, in which the Li plating samples with a Li loading of 0.5 mAh cm^{-2} were harvested after the Li/M cells were plated to 0.5 mAh cm^{-2} and striped to 1.0 V at 0.5 mA cm^{-2} for 10 cycles. On the pristine Cu foil, Li metal is plated naturally in the form of needle-like filaments, and the Li filaments are randomly and loosely piled (Fig. 4a). More importantly, the adhesion of Li plating to the Cu substrate is rather poor so that some Li deposits are irregularly dropped off the Cu surface (Fig. 4b). In contrast, Li metal is plated compactly and largely on the Sn-Cu foil and no Li dropping-off is observed (Fig. 4c and d). Of interest, the shape of Li plating is changed from loose needle-like filaments on

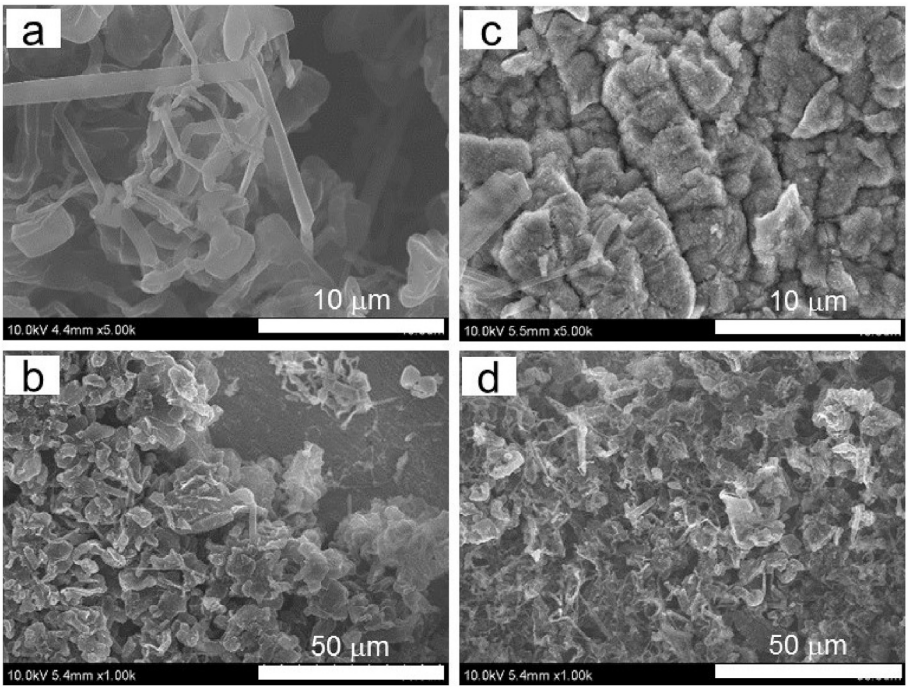

Fig. 4. SEM images of the surface of Li plating on Cu and Sn-Cu foils at different magnifications, which were obtained by plating Li to 0.5 mAh cm^{-2} after the cells were cycled at 0.5 mA cm^{-2} for 10 cycles. (a & b) on Cu foil, and (c & d) on Sn-Cu foil.

the Cu foil (Fig. 4a) to compact blocky pieces on the Sn-Cu foil (Fig. 4c). This can be attributed to two merits of the Sn-Cu substrate: (1) excellent lithiophilicity of Li-Sn alloy for uniform Li nucleation, and (2) enhanced adhesion of Li nuclei to the electrode substrate for growth of large Li granules. Compared with the blocky Li, the needle-like Li have much higher specific surface area and consequently are more reactive to the electrolyte components. The needle-like Li filaments are easy to become inactive "dead Li" once they are broken down and the broken Li segments are reacted with electrolyte components to form electron-insulating SEI around their surface. Therefore, the compact and blocky deposition of Li metal on the Sn-Cu foil is greatly beneficial to increasing the Li cycling efficiency and stability.

Fig. 5 indicates the cross-sectional views of Li plating on the Cu foil and Sn-Cu foil, respectively. On the Cu foil (Fig. 5a), there is a wide gap between the Li plating and Cu substrate, indicating poor adhesion of the Li plating to Cu substrate. These Li isolated by the gap are easily converted into "dead Li" if the gap is large enough to isolate Li from the Cu substrate and the isolated Li are fully wrapped by the electron-insulating SEI. In contrast, the Li plating is intimately deposited onto the Sn-Cu foil without significant gaps (Fig. 5b), and accordingly the Li metal exhibits higher CE and better cycling stability as a result of the excellent electrical contact between the Li plating and Sn-Cu substrate.

The improved adhesion of Li plating to electrode substrate by the pre-plated tin primer layer is also reflected in the Li/M cell's impedance. Fig. 6 compares ac-impedance spectra of two Li/M cells at the Li-plated state (having a Li loading of 0.5 mAh cm^{-2}). Typically, the ac-impedance spectrum of such cells shows three overlapped semicircles followed by a sloping straight line, which can be fitted by an equivalent circuit consisting of a bulk resistance (R_b), a surface layer resistance (R_{sl}), a contact resistance (R_c) between Li plating and electrode substrate, a charge-transfer resistance (R_{ct}), and a Weber impedance (W) sequentially in the order of frequency descending [23]. In the present case, response times of the R_{sl} and R_c are so close that they can hardly be separated. Therefore, a simplified equivalent circuit with the R_{sl} and R_c being merged into a $R_{sl\text{-}c}$, as indicated in the inset of Fig. 6, was proposed to analyze the observed impedance spectra. Using the simplified equivalent circuit, the value of each resistance element is fitted, showing that the Li/Sn-Cu cell has significantly smaller $R_{sl\text{-}c}$ and R_{ct} (i.e., 87 Ω and 121 Ω, respectively, versus 221 Ω and 180 Ω of the Li/Cu cell) although it has the same R_b (7.3 Ω) as the Li/Cu cell does. Here, the significantly smaller $R_{sl\text{-}c}$ of the Li/Sn-Cu cell excellently evidences that the pre-plated tin layer effectively enhanced the electrical contact between Li plating and electrode substrate. This result well agrees with our speculation that the tin primer layer is capable of enhancing the adhesion of Li plating to electrode substrate by functioning as an "electric glue" to electrically connect the Li plating and electrode substrate.

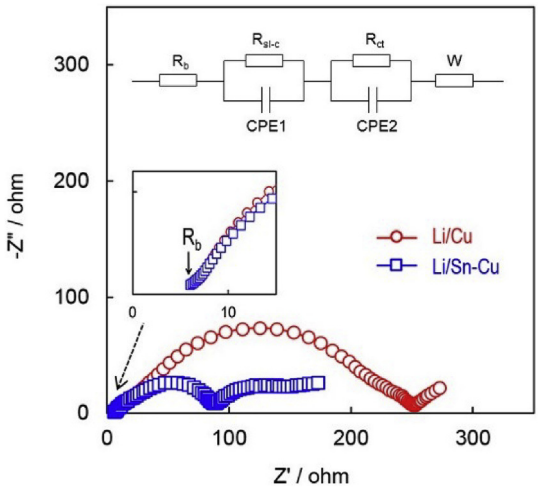

Fig. 6. Ac-impedance spectra of the Li/Cu and Li/Sn-Cu cells at Li-plated state (having a Li loading of 0.50 mAh cm^{-2}), in which the inset shows an equivalent circuit used for fitting the observed ac-impedance spectra.

The effect of the tin primer layer on the Li cycling performance is further examined in M/NCA cells. Fig. 7a shows voltage profiles of the first two cycles for three M/NCA cells (M = Li, Cu, and Sn-Cu, respectively), which were recorded at 0.1 mA cm^{-2} by charging the cell to 4.2 V and discharging to 3.0 V. Overall, three cells have very similar areal specific capacities and CEs (see the numbers in Fig. 7a). That is, the CE is 79.4%, 78.5, and 78.3% in the 1st cycle, and increases to 96.1%, 95.1, and 95.1% in the 2nd cycle for the Li/NCA, Cu/NCA, and Sn-Cu/NCA cells, respectively. As usual, the much lower CE in the 1st cycle is attributed to the irreversible capacities consumed mainly for two aspects of (1) the formation of SEI on the NCA particle surface and (2) the rearrangement of NCA crystalline structure, respectively [34]. Compared with the Li/NCA cell, the Cu/NCA and Sn-Cu/NCA cells show very small amount of extra irreversible capacities in the 1st charging as indicated in the inset in Fig. 7a, which can be attributed to the reduction of native oxides on the Cu foil for the Cu/NCA cell and to the formation of Li-Sn alloy for the Sn-Cu/NCA cell. Starting from the 3rd cycle, the current density is increased to 0.5 mA cm^{-2}, and the cells' capacity and CE are compared in Fig. 7b. It is observed that both the capacity retention and CE are decreased in the order of Li/NCA cell > Sn-Cu/NCA cell > Cu/NCA cell. In particular, the Cu/NCA cell was run only for about 30 cycles, and the Sn-Cu/NCA cell for about 80 cycles before their capacities declined to zero. It is of interest to find that the capacity fading rate of three cells roughly equals to "100-CE". For example, the averaged CE in Fig. 3c for Li plating on the Cu foil is

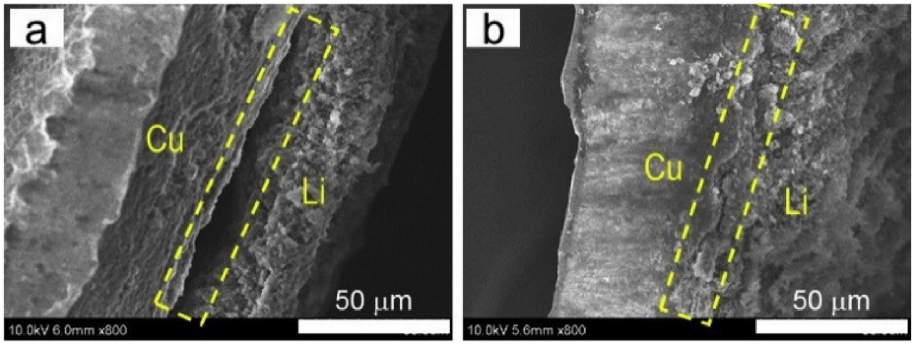

Fig. 5. SEM images of the cross-sectional view of the Li plating as described in Fig. 4. (a) on Cu foil, and (b) on Sn-Cu foil.

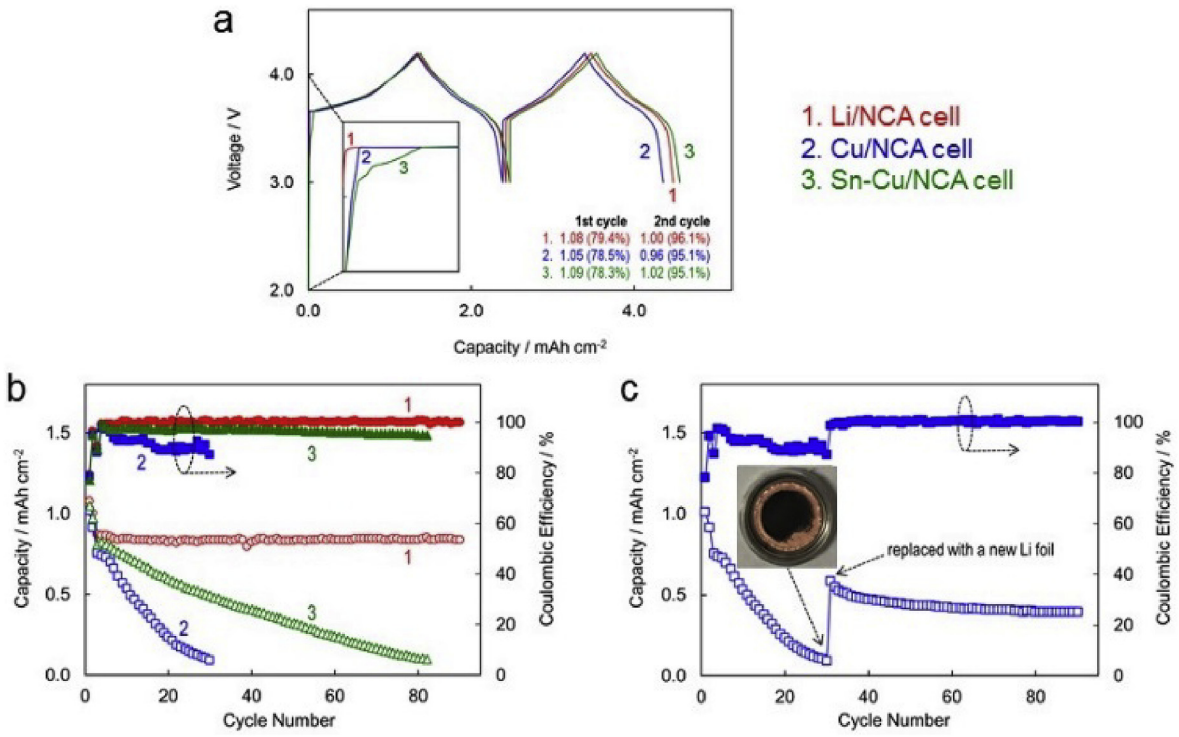

Fig. 7. Cycling performance of the M/NCA cells with different anode materials. (1) Li foil, (2) Cu foil, and (3) Sn-Cu foil. (a) Voltage profile of the 1st and 2nd cycles, in which the numbers indicate discharge capacity (mAh cm^{-2}) and coulombic efficiency (%), (b) plots of discharge capacity and coulombic efficiency vs. cycle number, and (c) capacity recovery of a dead Cu/NCA cell by replacing Cu foil with a fresh Li foil, where the inset shows a digital photo of dead Li particles on the Cu foil.

93%, and accordingly the capacity fading rate of the Cu/NCA cell in Fig. 7b is determined to be about 7% per cycle (=100−93%).

In order to understand the mechanism for fast capacity fading of the Cu/NCA cell, the dead cell was disassembled and the Cu foil was replaced with a fresh Li foil. As shown in the inset of Fig. 7c, there are numbers of powder-like dead Li, in a black color, on the Cu surface, and these dead Li are found to immediately evolve hydrogen when being in contact with water. Upon the replacement of the Cu foil by a fresh Li foil, more than half of the capacities are recovered and the CEs approach nearly 100% (see Fig. 7c). The above results reveal that the Li source for forming dead Li is originated from the NCA cathode, and that the fast capacity fading of the Cu/NCA cell is truly due to the loss of reversible Li^+ ions from the NCA cathode as a result of the low CE of Li cycling on the Cu substrate. The difference in the capacity retention between the Cu/NCA and Sn-Cu/NCA cells, as observed in Fig. 7b, evidently indicates the positive effect of the pre-plated tin primer layer on the Li cycling performance although the present results are still far away from the requirement for practically viable batteries. Finally, it should be noted that the electrode substrate is expected only to affect the nucleation of Li metal and the adhesion of resultant Li plating to the electrode substrate. The next growth of Li metal relies more on the electrolyte, which is beyond the scope of the present paper.

4. Conclusions

In summary, in this work we demonstrated the importance of electrode substrate in affecting the Li cycling performance, and proposed a simple approach for the modification of existing Cu current collector. By pre-plating a very thin tin layer onto the existing Cu foil, the Li metal can be first reacted with the Sn metal to form a Li-Sn alloy, and the next Li metal is cycled on the Li-Sn alloy surface, other than on the Cu substrate. Due to the chemistry similarity between Li metal and Li-Sn alloy, the resultant Li-Sn alloy is shown to behave as an “electrical glue” to electrically connect the Li plating and electrode substrate, which leads to considerably improved adhesion of Li plating to the electrode substrate and consequently increases the Li cycling efficiency and stability in the rechargeable lithium batteries. However, the electrode substrate is expected only to affect the nucleation of Li metal and the adhesion of Li plating to the electrode substrate, the next growth of Li metal relies more on the electrolyte. In order to make the “Li-free” batteries practically viable, suitable electrolyte must be developed in parallel with the modification of existing Cu substrate.

Acknowledgments

The authors are grateful to Drs. A. von Cresce and K. Xu for generously providing fluorethylene carbonate solvent, and to Dr. C. Lundgren for her critical reading of the manuscript and valuable comments.

References

[1] D. Lin, Y. Liu, Y. Cui, Reviving the lithium metal anode for high-energy batteries, Nat. Nano 12 (2017) 194–206.
[2] X.B. Cheng, R. Zhang, C.Z. Zhao, Q. Zhang, Toward safe lithium metal anode in rechargeable batteries: a review, Chem. Rev. 117 (2017) 10403–10473.
[3] B.J. Neudecker, N.J. Dudney, J.B. Bates, “Lithium-free” thin-film battery with in situ plated Li anode, J. Electrochem. Soc. 147 (2000) 517–523.
[4] J.F. Qian, B.D. Adams, J.M. Zheng, W. Xu, W.A. Henderson, J. Wang, M.E. Bowden, S.C. Xu, J.Z. Hu, J.G. Zhang, Anode-free rechargeable lithium metal batteries, Adv. Func. Mater. 26 (2016) 7094–7102.
[5] L. Suo, Y.S. Hu, H. Li, M. Armand, L. Chen, A new class of solvent-in-salt electrolyte for high-energy rechargeable metallic lithium batteries, Nat. Commun. 4 (2013) 1481.
[6] J. Qian, W.A. Henderson, W. Xu, P. Bhattacharya, M. Engelhard, O. Borodin, J.G. Zhang, High rate and stable cycling of lithium metal anode, Nat. Commun. 6 (2015) 6362.
[7] J.M. Zheng, P.F. Yan, D.H. Mei, M.H. Engelhard, S.S. Cartmell, B.J. Polzin,

C.M. Wang, J.G. Zhang, W. Xu, Highly stable operation of lithium metal batteries enabled by the formation of a transient high-concentration electrolyte layer, Adv. Energy Mater. 6 (2016) 1502151.
[8] Y. Yamada, A. Yamada, Review—superconcentrated electrolytes for lithium batteries, J. Electrochem. Soc. 162 (2015) A2406–A2423.
[9] H. Wang, M. Matsui, H. Kuwata, H. Sonoki, Y. Matsuda, X.F. Shang, Y. Takeda, O. Yamamoto, N. Imanishi, A reversible dendrite-free high-areal-capacity lithium metal electrode, Nat. Commun. 8 (2017) 15106.
[10] E. Markevich, G. Salitra, F. Chesneau, M. Schmidt, D. Aurbach, Very stable lithium metal stripping-plating at a high rate and high areal capacity in fluoroethylene carbonate-based organic electrolyte solution, ACS Energy Lett. 2 (2017) 1321–1326.
[11] J.M. Zheng, M.H. Engelhard, D.H. Mei, S.H. Jiao, B.J. Polzin, J.G. Zhang, W. Xu, Electrolyte additive enabled fast charging and stable cycling lithium metal batteries, Nat. Energy 2 (2017) 17012.
[12] X.Q. Zhang, X.B. Cheng, X. Chen, C. Yan, Q. Zhang, Fluoroethylene carbonate additives to render uniform Li deposits in lithium metal batteries, Adv. Funct. Mater. 27 (2017) 1605989.
[13] R. Miao, J. Yang, Z. Xu, J. Wang, Y. Nuli, L. Sun, A new ether-based electrolyte for dendrite-free lithium-metal based rechargeable batteries, Sci. Rep. 6 (2016) 21771.
[14] H.L. Yu, J.N. Zhao, L.B. Ben, Y.J. Zhan, Y.D. Wu, X.J. Huang, Dendrite-free lithium deposition with self aligned columnar structure in a carbonate-ether mixed electrolyte, ACS Energy Lett. 2 (2017) 1296–1302.
[15] W. Xu, J.L. Wang, F. Ding, X.L. Chen, E. Nasybutin, Y.H. Zhang, J.G. Zhang, Lithium metal anodes for rechargeable batteries, Energy Environ. Sci. 7 (2014) 513–537.
[16] J. Qian, W. Xu, P. Bhattacharya, M. Engelhard, W.A. Henderson, Y. Zhang, J.G. Zhang, Dendrite-free Li deposition using trace-amounts of water as an electrolyte additive, Nano Energy 15 (2015) 135–144.
[17] H. Wu, Y. Cao, L. Geng, C. Wang, In-situ formation of stable interfacial coating for high performance lithium metal anodes, Chem. Mater. 29 (2017) 3572–3579.
[18] X.B. Cheng, C. Yan, H.J. Peng, J.Q. Huang, S.T. Yang, Q. Zhang, Sulfurized solid electrolyte interphases with a rapid Li^+ diffusion on dendrite-free Li metal anodes, Energy Storage Mater. (2017), https://doi.org/10.1016/j.ensm.2017.03.008 in press.
[19] X. Ji, D.Y. Liu, D.G. Prendiville, Y. Zhang, X. Liu, G.D. Stucky, Spatially heterogeneous carbon-fiber papers as surface dendrite-free current collectors for lithium deposition, Nano Today 7 (2012) 10–20.
[20] R. Mukherjee, A.V. Thomas, D. Datta, E. Singh, J. Li, O. Eksik, V.B. Shenoy, N. Koratkar, Defect-induced plating of lithium metal within porous graphene networks, Nat. Commun. 5 (2014) 3710.
[21] R. Zhang, X.B. Cheng, C.Z. Zhao, H.J. Peng, J.L. Shi, J.Q. Huang, J.F. Wang, F. Wei, Q. Zhang, Conductive nanostructured scaffolds render low local current density to inhibit lithium dendrite growth, Adv. Mater. 28 (2016) 2155–2162.
[22] R. Zhang, X.R. Chen, X. Chen, X.B. Cheng, X.Q. Zhang, C. Yan, Q. Zhang, Lithiophilic sites in doped graphene guide uniform lithium nucleation for dendrite-free lithium metal anodes, Ang. Chem. Intern. Ed. 56 (2017) 7764–7768.
[23] S.S. Zhang, X.L. Fan, C.S. Wang, Efficient and stable cycling of lithium metal enabled by a conductive carbon primer layer, Sustain. Energy Fuels (2018), https://doi.org/10.1039/C7SE00391A in press.
[24] A.R.O. Raji, R. Villegas Salvatierra, N.D. Kim, X. Fan, Y. Li, G.A.L. Silva, J. Sha, J.M. Tour, Lithium batteries with nearly maximum metal storage, ACS Nano 11 (2017) 6362–6369.
[25] C. Zhang, Z. Huang, W. Lv, Q. Yun, F. Kang, Q.H. Yang, Carbon enables the practical use of lithium metal in a battery, Carbon 123 (2017) 744–755.
[26] J.R. Henry, Electroless (autocatalytic) plating, Metal. Finish 97 (1999) 431–442.
[27] MG Liquid Tin 421 Technical Data Sheet, http://www.mgchemicals.com/downloads/tds/tds-421-l.pdf, Accessed on 9/13/2017.
[28] Cu-Sn phase diagrams & computational thermodynamics, https://www.metallurgy.nist.gov/phase/solder/cusn.html, accessed on 11/20/2017.
[29] A. Pei, G.Y. Zheng, F.F. Shi, Y.Z. Li, Y. Cui, Nanoscale nucleation and growth of electrodeposited lithium metal, Nano Lett. 17 (2017) 1132–1139.
[30] A.N. Dey, Electrochemical alloying of lithium in organic electrolytes, J. Electrochem. Soc. 118 (1971) 1547–1549.
[31] M. Winter, J.O. Besenhard, Electrochemical lithiation of tin and tin-based intermetallics and composites, Electrochim. Acta 45 (1999) 31–50.
[32] N. Tamura, R. Ohshita, M. Fujimoto, S. Fujitani, M. Kamino, I. Yonezu, Study on the anode behavior of Sn and Sn–Cu alloy thin-film electrodes, J. Power Sources 107 (2002) 48–55.
[33] N. Tamura, R. Ohshita, M. Fujimoto, M. Kamino, S. Fujitani, Advanced structures in electrodeposited tin base negative electrodes for lithium secondary batteries, J. Electrochem. Soc. 150 (2003) A679–A683.
[34] S.S. Zhang, K. Xu, T.R. Jow, Formation of solid electrolyte interface in lithium nickel mixed oxide electrodes during the first cycling, Electrochem. Solid State Lett. 5 (2002) A92–A94.